Voltage-Driven Molecular Photoelectrocatalysis of Water Oxidation

Koushik Barman,[†,*] Gaukhar Askarova,[†,§] Rahul Somni,[‡] Guoxiang Hu,[¶,‡,*] and Michael V. Mirkin[†,#,*]

† Department of Chemistry and Biochemistry, Queens College-CUNY, Flushing, NY 11367, USA.

§ The Graduate Center of CUNY, New York, NY 10016, USA.

‡ School of Chemistry and Biochemistry, Georgia Institute of Technology, Atlanta, GA 30332, USA.

¶ School of Materials Science and Engineering, Georgia Institute of Technology, Atlanta, GA 30332, USA.

Advanced Science Research Center at The Graduate Center, CUNY; New York, NY 10031, USA.

Corresponding Author

E-mail: koushik.barman2@gmail.com, emma.hu@mse.gatech.edu, mmirkin@qc.cuny.edu

ABSTRACT

Molecular photocatalysis and photoelectrocatalysis have been widely used to conduct oxidation-reduction processes ranging from fuel generation to electroorganic synthesis. We recently showed that electrostatic potential drop across the double layer contributes to the driving force for electron transfer (ET) between a dissolved reactant and a molecular catalyst immobilized directly on the electrode surface. In this Article, we report voltage-driven molecular photoelectrocatalysis with a prevalent homogeneous water oxidation catalyst, (bpy)Cu(II), which was covalently attached to the carbon surface and exhibited photocatalytic activity. The strong potential dependence of the photooxidation current suggests that the electrostatic potential drop across the double layer contributes to the driving force for ET between a water molecule and the excited state of surface-bound (bpy)Cu(II). Scanning electrochemical microscopy (SECM) was used to analyze the products and determine faradaic efficiencies for the generation of oxygen and hydrogen peroxide. Unlike electrocatalytic water oxidation by (bpy)Cu(II) in the dark, which produces only O_2, the voltage-driven photooxidation includes an additional $2e^-$ pathway generating H_2O_2. DFT calculations show that the applied voltage and the presence of light can alter the activation energy for the rate-determining water nucleophilic attack steps, thereby increasing the reaction rate of photooxidation of water and opening the $2e^-$ pathway. These results suggest a new route for designing next-generation hybrid molecular photo(electro)catalysts for water oxidation and other processes.

INTRODUCTION

A number of applications of interfacial photoelectrochemistry (i.e., generation of photocurrent on photoelectrode surfaces to promote chemical transformations[1]) and electrophotochemistry (i.e., photoelectrochemical catalyst-mediated electrolysis[2]) in energy conversion and synthetic chemistry have been reported over the past few decades.[3,4] These approaches have been used to generate potent oxidizing and reducing agents at less extreme electrode potentials by combining the power of electrical and photochemical energy.[5] There is considerable interest in development of molecular photoelectrocatalysts (i.e., the molecules simultaneously acting as light absorbers and electrocatalysts) for fuel generation[6] and water splitting[7-9] because they offer substantial tunability without the need for complex engineering and characterization of active sites essential for heterogeneous electrocatalysts. The excited states of electron donors and acceptors have been used as "super-reductants" and "super-oxidants", respectively, in photoinduced hydrogen evolution reaction (HER) and oxygen evolution reaction (OER).[10]

Similar to molecular electrocatalysts,[11,12] a molecular photoelectrocatalyst is electrochemically regenerated at the electrode surface following its photocatalytic reaction with redox species dissolved in solution. In reported experiments, the applied electrode potential only induced oxidation/reduction of photoelectrocatalyst and did not drive a bimolecular catalytic reaction, which, therefore, required a strong oxidizing and reducing chemical agent; e.g., a molecular photoelectrocatalyst for OER must be sufficiently potent to oxidize water.[7,10,12]

Molecular (photo)electrocatalysts for water splitting typically based on transition-metal complexes are usually homogeneous (i.e., dissolved in solution).[3,6,8-10,12-17] Surface attachment of a molecular catalyst can enhance its activity, reduce the catalyst loading and simplify its recycling.[18-22] Recent studies focused on the advantages of combining molecular catalysts and

electrocatalysts into hybrid systems,[23-28] including several reports from the Surendranath group, in which direct coupling of catalysts to carbon electrodes produced tunable heterogeneous catalysts with molecularly well-defined active sites.[29-31]

We showed recently that the potential drop can contribute to the driving force for the ET between an immobilized molecular catalyst situated within the electric double layer (EDL) and dissolved reactant molecules.[32-34] In voltage-driven catalysis, a fraction of the applied potential drops between the electrode and the immobilized molecular catalyst, inducing oxidation/reduction of the catalyst, while the potential drop between the catalyst and the dissolved reactant drives the electrocatalytic process.[32] In this way, the applied electrode potential can increase the oxidizing (or reducing) ability of a surface-bound molecular catalyst and allow it to accelerate the rates of charge-transfer processes, which it normally would not be able to catalyze.[33] Here we introduce a new concept – voltage-driven molecular photoelectrocatalysis, in which the applied electrode potential contributes to the driving force for a molecular photocatalytic process. A 2,2'-bipyridine copper—(bpy)Cu(II)—electrocatalyst for OER reported by the Mayer group[17] exhibited potential-dependent photoelectrocatalytic activity for water oxidation when attached directly to the carbon electrode surface. We used this process as a model system to develop a new approach to hybrid molecular photoelectrocatalysis and show that the same voltage-driven molecular catalyst can enable different reaction pathways in the dark and under illumination.

RESULTS & DISCUSSION

Voltage-driven molecular catalysis of water oxidation at a (bpy)Cu-modified carbon electrode. (bpy)Cu was covalently attached to the carbon surface using a literature protocol[35] (see Experimental section). First, a monolayer of bipyridine molecules was formed on a glassy carbon electrode (GCE) using diazonium grafting method in the presence of

2,2-diphenyl-1-picrylhydrazyl (DPPH), as described previously,[36] to avoid multilayer film formation. To produce a sub-monolayer coverage of (bpy)Cu, the bpy-modified electrode was immersed in DMF solution of copper nitrate overnight[35] (see Experimental section). Cyclic voltammograms (CVs; Figure 1) of Cu-bpy modified GCE in 0.1 M phosphate buffer saline (PBS) at pH 7 show a pair of reversible Cu(II)/Cu(I) oxidation/reduction peaks with the mid-peak potential, $E_{1/2}$ = -0.16 V vs. Ag/AgCl reference, whereas the reported $E_{1/2}$ for dissolved Cu-bpy is -0.31 V vs. Ag/AgCl.[17] The background-subtracted cathodic peak current was directly proportional to the scan rate (the inset in Figure 1), and the surface coverage of (bpy)Cu, $\Gamma_{Cu\text{-}bpy}$ = 4.8 pmol/cm^2, was calculated by integrating the area under the cathodic peak after background subtraction (Figure S1). This value corresponds to much less than the full monolayer coverage (~6 × 10^{-10} mol·cm^{-2} [37]). Accordingly, the CVs of 0.5 mM ferricyanide in 0.1 M PBS (pH 7) recorded at the same GCE before (Figure S2A, red curve) and after (bpy)Cu immobilization on its surface (Figure S2A, blue curve) show only a slight blocking effect. By contrast, very strong blocking of ferricyanide ET can be seen in a CV of GCE coated with a thick film of (bpy)Cu, which was deposited on a bipyridine multilayer produced by diazonium grafting in absence DPPH (Figure S2B).

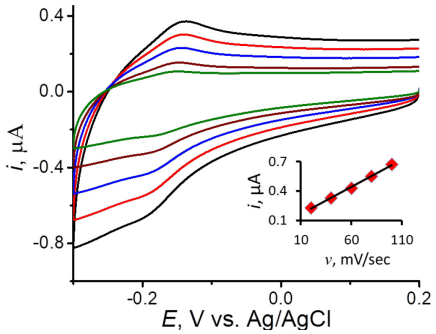

Figure 1. Cyclic voltammograms of (bpy)Cu-modified 3-mm-diameter GCE recorded in 0.1 M PBS (pH 7) at different scan rates. ν, mV/s = 20 (green), 40 (brown), 60 (blue), 80 (red), and 100 (black). Inset: scan rate dependence of the cathodic peak current.

The water oxidation catalysis at (bpy)Cu-modified GCE electrodes is shown in Figure 2. A voltammogram obtained at the GCE coated with a sub-monolayer of (bpy)Cu in 0.1 M PBS (pH 7; red curve in Figure 2A) shows the water oxidation current much higher than that at the bare GCE (black curve). The current onset occurs at ~0.5 V, and the current continues to increase over a wide potential range (~800 mV), which cannot be attributed to direct oxidation of water on the bare carbon surface because the current produced by this process (Figure 2A, black curve) is much lower than that at the modified GCE. This behavior is characteristic of voltage-driven molecular catalysis.[32,33] An *i-t* curve of (bpy)Cu in PBS (Figure S3A) shows negligible homogeneous catalysis of water oxidation at pH 7. The catalytic *i-t* response of (bpy)Cu-GCE for OER is stable on the minutes to hours time scale in either 0.1 M PBS of pH 7 (Figure S4, curve 1) or 0.1 M KOH (Figure S4, curve 2).

The very low water oxidation activity of multilayer (bpy)Cu films (Figure 2B) suggests that only the first catalytic molecular monolayer located within EDL, where the potential drop enhances the oxidizing power of (bpy)Cu, exhibits a significant catalytic activity in pH 7 PBS solution. The lower water oxidation current points to the blocking effect of the thick (bpy)Cu film. (bpy)Cu was also immobilized on the surface of a carbon nanoelectrode (CNE; Figure S5) and exhibited a much faster apparent rate of catalytic OER with the current density reaching

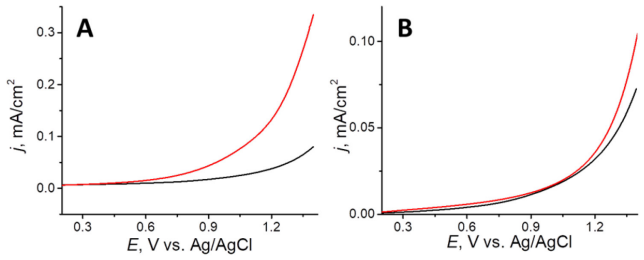

Figure 2. Voltammograms of water oxidation at (bpy)Cu-GCE (red curve) and bare GCE (black) in 0.1 M PBS (pH 7). v = 20 mV/s. GCE was modified with a sub-monolayer (A) and multilayer (B) (bpy)Cu film.

>1 A/cm^2. This high activity is due to a large apparent coverage of the porous CNE surface by (bpy)Cu. Similar responses were previously observed at CNEs modified by other molecular catalysts.[32,33] A bare CNE surface is inactive towards water oxidation (Figure S5A, curve 1).

Voltage-driven molecular photoelectrocatalysis of water oxidation by (bpy)Cu. The comparison of voltammograms recorded in the same solution and at the same (bpy)Cu-GCE in the dark (Figure 3A, blue curve) and under illumination (red curve) suggests that the water oxidation rate can be significantly enhanced by photoelectrocatalysis. The magnitude of the photooxidation current can be evaluated from the amplitude of chopped-light transients at different applied potentials (Figure 3B), which show the increase in both the dark current (in agreement with Figure 2A) and the amplitude of the photocurrent with *E* over a several hundred

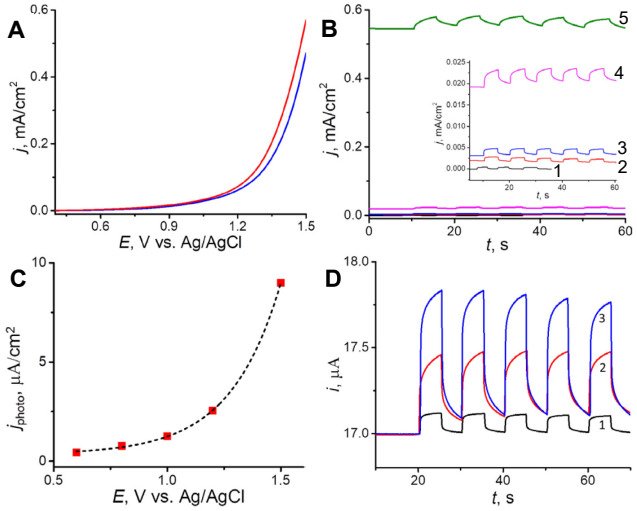

Figure 3. Photoelectrocatalysis of water oxidation by (bpy)Cu. (A) Voltammograms recorded at a (bpy)Cu-GCE with (red curve) and without (blue curve) light. v = 5 mV/s. (B) Chopped-light current transients of water oxidation at a (bpy)Cu-GCE obtained in the same solution at different potentials, *E,* V vs. Ag/AgCl = 0.6 (1), 0.8 (2), 1.0 (3), 1.2 (4), 1.5 (5). Inset: zoom in of the four *j-t* curves obtained at lower potentials. (C) Potential dependence of the photocurrent amplitude obtained from the chopped-light transients in panel B. (D) Chopped-light current transients obtained at different light intensities and *E* = 1.3 V. The light source power (W) was: 150 (1), 200 (2), and 250 (3). Solution was 0.1 M PBS (pH 7).

mV potential range. The corresponding potential dependence of the photocurrent (Figure 3C) is indicative of voltage-driven molecular photoelectrocatalysis of water oxidation by surface-bound (bpy)Cu. The applied voltage apparently contributes to the driving force for the bimolecular photoelectrochemical reaction. Variable light intensity chopped-light current transients obtained at a constant value of the applied potential (1.3 vs. Ag/AgCl) are shown in Figure 3D. As expected, the photooxidation current increases with light intensity. No photocurrent transients were observed at a bare GCE without (bpy)Cu attached to its surface (Figure S3).

SECM detection of water oxidation products at (bpy)Cu-GCE under illumination and in the dark. We used the substrate generation/tip collection (SG/TC; Scheme 1) mode of scanning electrochemical microscopy (SECM) to quantify the products and evaluate faradaic efficiency for the processes occurring during the water oxidation at (bpy)Cu-GCE under illumination and in the dark. A (bpy)Cu-modified GCE was used as a substrate electrode in pH 7 0.1 M PBS solution. If the tip potential (E_T) is negative, both O_2 and H_2O_2 are reduced at the tip (A), whereas only oxidation of H_2O_2 occurs at the tip when E_T is positive (B).

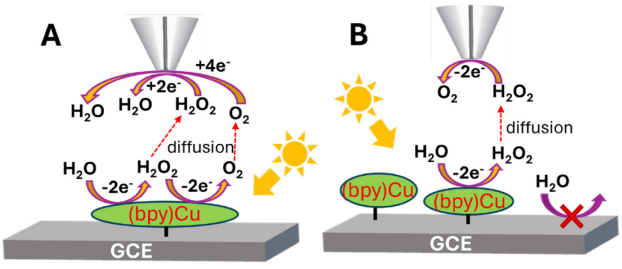

Scheme 1. Schematic representation of SG/TC SECM measurements of voltage-driven water oxidation by (bpy)Cu. (A) H_2O_2 produced by photooxidation of water at (bpy)Cu-GCE can either diffuse away from the substrate surface or get further oxidized to produce O_2. Both oxidation products are reduced at the negatively biased SECM tip. (B) H_2O_2 produced at the substrate is oxidized at the positively biased tip. No water oxidation occurs at the catalytically inert carbon surface. The experiments were carried out either under illumination or in the dark (not shown).

Three tip current vs. time (i_T - t) curves in Figure 4A were obtained with the same 5-μm-radius Pt tip positioned 5 μm above the (bpy)Cu-GCE surface and biased at E_T = -0.65 V vs. Ag/AgCl to reduce O_2 and H_2O_2. At the substrate potential, E_S = 0 V (curve 1), no water oxidation occurred at its surface, and the tip current (i_T = -2.4 nA) was due to the reduction of dioxygen dissolved in solution. A much larger current (i_T = -11.5 nA) was recorded at E_S =1.3 V (curve 2) due to the reduction of O_2 (and possibly H_2O_2) generated at the (bpy)Cu-GCE in the dark. The difference between the tip current values in curve 3 (-13.4 nA; measured at the same E_S = 1.3 V but under illumination) and curve 2 represents the contribution of photogenerated O_2 and H_2O_2 species to i_T. The same quantity can be evaluated from the amplitude of the photocurrent transients (Figure 4B), which increases from curve 1 to curve 3 as the E_S becomes more positive. The flux of photogenerated dioxygen also increases with the light intensity (Figure 4C).

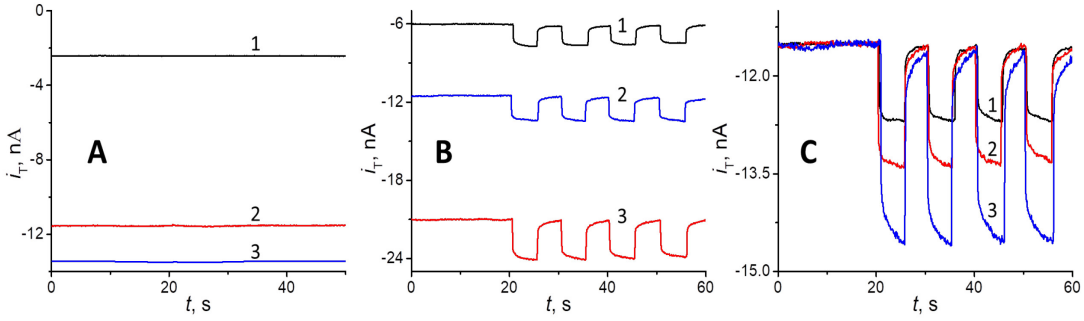

Figure 4. Probing water oxidation at the (bpy)Cu-GCE substrate in 0.1 M PBS with SECM. (A) i_T-t curves recorded at a 5 μm-radius Pt tip (E_T = -0.65 V) positioned 5 μm above the substrate surface. E_S, V vs. Ag/AgCl = 0 (1), 1.3 (2, 3). Curves 1 and 2 were recorded in the dark, and curve 3 – under illumination. (B) Chopped-light current transients obtained under the same conditions as in (A) at different substrate potentials. E_S, V vs. Ag/AgCl = 1.1 (1), 1.3 (2), and 1.5 (3). The light source power was 200 W. (C) Chopped-light current transients obtained at different light intensities and E_S = 1.3 V. The light source power (W) was: 150 (1), 200 (2), and 250 (3).

Unlike the i_T-t curves in Figure 4, the tip current of H_2O_2 oxidation measured in the dark (Figure 5A) is immeasurably low at any E_S value, indicating that oxygen is the only product of voltage-driven water electrooxidation at (bpy)Cu-GCE. The current of H_2O_2 oxidation appears at the tip (at the same E_T = 0.8 V vs. Ag/AgCl) when the substrate is illuminated, and its magnitude increases with light intensity (Figure 5A). This observation suggests that the electrophotooxidation of water by (bpy)Cu(II) includes an additional $2e^-$ pathway generating H_2O_2. The amplitude of the photocurrent transients is much smaller that the dark current value, indicating that the $4e^-$ pathway remains dominant under moderate light intensities used in our experiments. Interestingly, the amplitude of the chopped-light transients decreases with increasing E_S value (from curve 3 to curve 1 in Figure 5B). We attribute this behavior to rapid oxidation of H_2O_2 at (bpy)Cu-GCE whose rate increases when the substrate potential becomes more positive.

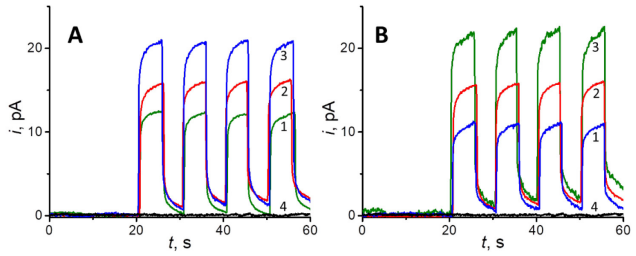

Figure 5. Hydrogen peroxide flux generated at the (bpy)Cu-GCE substrate in 0.1 M PBS is collected at the SECM tip biased at 0.8 V vs. Ag/AgCl. A 5 μm-radius Pt tip was positioned 5 μm above the (bpy)Cu-GCE surface. (A) Chopped-light current transients obtained at the same substrate potential, E_S = 1.3 V, and different light intensities. The light source power (W) was: 150 (1), 200 (2), and 250 (3). (B) Chopped-light current transients obtained with the constant light source power of 200 W and different E_S values. E_S, V vs. Ag/AgCl = 1.5 (1), 1.3 (2), and 1.1 (3). Curves 4 show same chopped-light current transient obtained with a bare GCE substrate biased at 1.1 V and the light source power 200 W. The 2 pA potentiostat offset current is subtracted from all data.

Finite-element simulations (Supporting Information) were conducted to evaluate the generated oxygen flux and faradaic efficiency from the measured tip and substrate currents. To isolate the contribution of oxygen generated in the dark to the tip current, i_T, we subtracted the current due to the reduction of dissolved oxygen (-2.4 nA) from the total measured tip current (-11.5 nA; Figure 4A, curve 2), yielding the value of -9.1 nA. This tip current corresponds to the oxygen flux generated on the substrate, 0.34 nmol/cm²·s, as determined from the SG/TC SECM COMSOL model (Supporting Information). Using this flux value (0.34 nmol/cm²·s), the corresponding substrate current due to oxygen generation was calculated to be 9.3 μA. Based on this value and the total measured substrate current of 17 μA, the faradaic efficiency for OER at the (bpy)Cu-GCE surface in the dark was calculated to be 54.7%.

Under illumination, the total tip current, i_T = -13.4 nA (Figure 4A, curve 3), and the tip current due to the reduction of substrate-generated oxygen is -11 nA. The corresponding oxygen flux on the substrate surface is 0.43 nmol/cm²·s. Using this flux value and the total substrate current of 17.4 μA, the faradaic efficiency for OER under illumination was calculated to be 67.4%. The tip currents of H_2O_2 oxidation (Figure 5) are several orders of magnitude lower than i_T of oxygen reduction (Figure 4); thus, the faradaic efficiency for H_2O_2 photogeneration is much lower than that for OER.

DFT calculations of photoassisted voltage-driven water oxidation by Cu-bpy modified GCE. Recent DFT calculations revealed that the potential drop between surface-bound redox species and dissolved reactant molecules can contribute to the driving force for a catalytic outer-sphere or inner-sphere ET reaction.[32-34] Here, we calculated the plane-averaged electrostatic potentials for (bpy)Cu-GCE at different values of the electrode potential. As shown in Figure 6, the electrostatic potential drops on both sides of the attached (bpy)Cu. This agrees with the

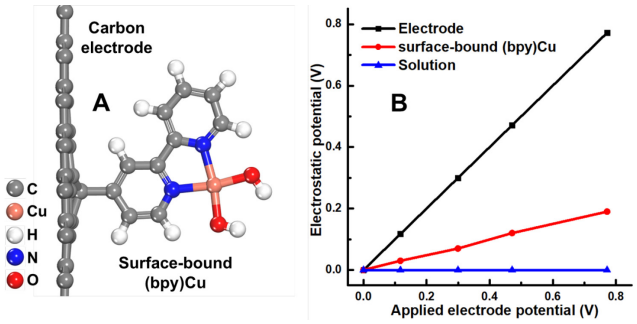

Figure 6. The optimized atomic structure of surface-bound (bpy)Cu (A) and calculated plane-averaged electrostatic potentials of the carbon electrode, surface-bound (bpy)Cu, and solution as a function of the applied electrode potential, E vs. E_{PZC} (B).

experimental observation that the mid-peak potential of surface-bound (bpy)Cu is more positive than that of (bpy)Cu dissolved in solution (Figure 1). Specifically, about 3/4 of the applied potential drops between the electrode and surface-bound (bpy)Cu, while the remaining 1/4 of it drops between surface-bound (bpy)Cu and solution. This 1/4 of the potential drop, thus, provides an additional driving force for (photo)electrooxidation of water.

The mechanism of water oxidation catalyzed by (bpy)Cu involves the rate-determining oxygen-oxygen bond formation through the water nucleophilic attack.[38,39] As shown in Figure 7, a (bpy)Cu(OH)(=O) intermediate is first formed at positive potentials. Then, a nucleophilic water molecule attacks the oxo group of the intermediate, which leads to the formation of an oxygen-oxygen σ bond and the breaking of one of the copper-oxygen π bonds. Here, the copper center is electrophilic to accept the *p* electrons from the oxo ligand. After the oxygen-oxygen bond formation, a copper-hydroperoxide species is generated, which undergoes further oxidation to release O_2. Besides the $4e^-$ water oxidation to O_2, $2e^-$ water oxidation could occur through a second water nucleophilic attack to produce H_2O_2.

We calculated the activation energy of the rate-determining oxygen-oxygen bond formation step for (bpy)Cu-GCE at different electrode potentials. Figures 8A and 8B show the atomic

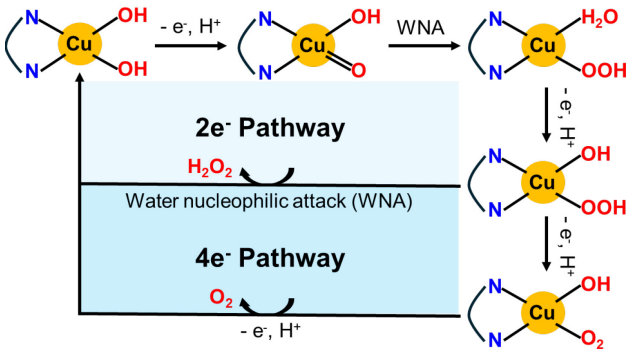

Figure 7. Catalytic mechanisms for the 2e⁻ water oxidation to H_2O_2, and 4e⁻ water oxidation to O_2.

structures of surface-bound (bpy)Cu before and after the oxygen-oxygen bond formation, respectively. The activation energy is as high as 1.65 eV when the applied electrode potential is low (Figure 8C); however, as the applied potential becomes more positive, the activation energy decreases and a low activation energy of 0.32 eV can be achieved with the applied electrode of 0.77 V (vs. E_{PZC}). This finding is consistent with the experimental voltammograms of water oxidation at (bpy)Cu-GCE (Figure 2), where the current continues to increase over a wide potential range, and the reaction rate becomes faster at higher anodic potentials.

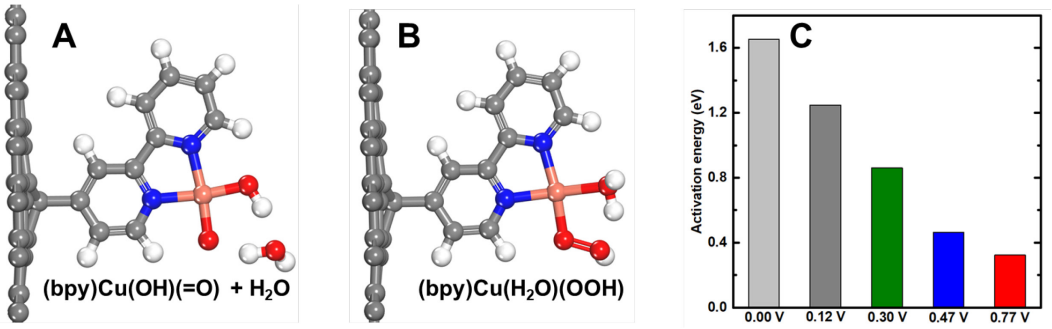

Figure 8. Water oxidation electrocatalysis by surface-bound (bpy)Cu. (A) Structure of the (bpy)Cu(OH)(=O) intermediate. (B) Oxygen-oxygen bond formation through the water nucleophilic attack. (C) Activation energy of the rate-determining oxygen-oxygen bond formation step as a function of E (vs. E_{PZC}).

The correlation between the activation energy of the oxygen-oxygen bond formation and the partial positive charge on the copper center revealed by electronic structure analysis can be explained by the water nucleophilic attack mechanism, where the metal center is electrophilic to accept electrons, and a more positive charge leads to a higher reaction rate. Thus, the partial positive charge on the metal center can be used as a descriptor for the reaction rate of the water nucleophilic attack.

Excited state calculations were performed to understand the effects of light on the reaction rate and pathway. We found a more positive charge on the copper center for the excited state of (bpy)Cu, which is attributed to the strong visible light absorption and metal-to-ligand charge transfer (MLCT) transition.[40] Moreover, the positive charge increases as the applied electrode potential become more positive, similar to the voltage-driven molecular catalysis in the dark (Figure 9). Thus, the higher water oxidation photocurrent is due to the more positive charge on the metal center and higher reaction rate of the rate-determining water nucleophilic attack. Likewise, the light-induced water oxidation to H_2O_2 is related to the increase in the reaction rate of the second water nucleophilic attack step of the $2e^-$ pathway (Figure 7). It should be noted that

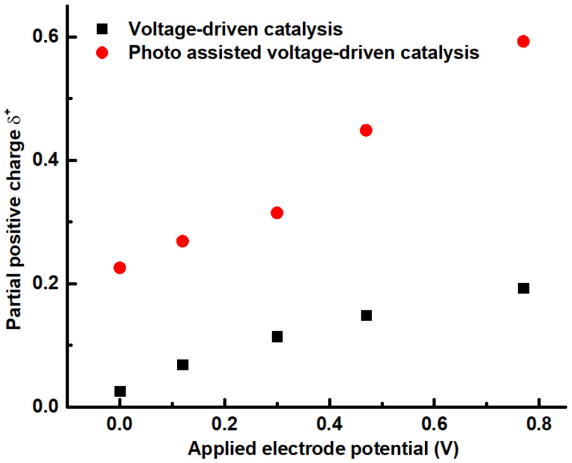

Figure 9. Partial positive charge on the copper center of the surface-bound (bpy)Cu as a function of E (vs. E_{PZC}) in the absence of light (black squares) and in the presence of light (red circles).

due to the complexity of the electrochemical interface, performing simulations with explicit solvation models would be useful to further confirm the effect of Cu partial charge. Taken together, our calculations suggest that the reaction rate and pathway of the voltage-driven molecular photoelectrocatalysis of water oxidation by surface-bound (bpy)Cu can be effectively tuned by the applied bias and light through reducing the activation energy for the rate-determining water nucleophilic attack steps.

CONCLUSION

In summary, a new catalytic process is reported in this Article – voltage-driven molecular photoelectrocatalysis – in which the applied potential contributes to the driving force for ET between dissolved species and photoelectrocatalyst directly attached to the electrode surface. We used water oxidation by (bpy)Cu in neutral aqueous solution as a model experimental system. When covalently attached to a carbon surface, this species exhibits both voltage-driven molecular electrocatalysis and photoelectrocatalysis, thus enabling the study of mechanistic differences between these two processes, including an additional $2e^-$ pathway appearing under illumination. DFT calculations showed that the applied voltage and light can alter the activation energy for the rate-determining water nucleophilic attack steps, thereby increasing the photooxidation reaction rate and opening the $2e^-$ pathway. The combination of electrochemical driving force and photoexcitation can enable a molecular photocatalyst to accelerate the rates of charge-transfer processes, which it normally would not be able to catalyze, and have important implications for energy conversion and photoelectrosynthesis.

EXPERIMENTAL SECTION

Chemicals and materials. $Cu(NO_3)_2 \cdot 3H_2O$, DMF, 2,2-diphenyl-1-picrylhydrazyl,

sodium nitrite, nitrosyl tetrafluoroborate, $TBABF_4$, and KOH were purchased from Sigma-Aldrich, and 4-Amino-2,2'-bipyridine was from Biosynth. Sodium phosphate dibasic (Sigma-Aldrich, 99.95% trace metals basis) and sodium phosphate monobasic (anhydrous, Sigma-Aldrich, 99.998% trace metals basis) were used to make 0.1 M phosphate buffer (pH 7.2). All aqueous solutions were prepared using water from Milli-Q Advantage A10 system (Millipore Corp.) equipped with Q-Gard T2 Pak, a Quantum TEX cartridge, and a VOC Pak with total organic carbon (TOC) ≤ 3 ppb.

Electrochemical instrumentation and procedures. Electrochemical experiments were carried out using a CHI 760E bipotentiostat (CH Instruments) inside a Faraday cage. In a three-electrode setup, either a 3 mm diameter GCE (CH Instruments) or a CNE was used as a working electrode, a Pt wire as a counter electrode, and a commercial Ag/AgCl (1 M KCl) as a reference electrode.

For photo-electrochemical experiments, the optical setup (Newport Corporation) consisted of an OPS-A500 500 W power supply, a 250 W HgXe lamp, and an IR cutoff FSQ-KG3 glass filter (Newport) was used to minimize sample heating during the experiment.

Fabrication of carbon nanoelectrodes. CNEs with the tip radii ~50 nm were prepared as reported previously.[41] Briefly, nanopipettes were produced by pulling quartz capillaries (1.0 mm o.d., 0.5 mm i.d.; Sutter Instrument Company) with a laser pipette puller (P-2000, Sutter Instruments). Carbon was deposited onto the inner pipette wall by chemical vapor deposition (CVD) at 900°C, using methane as carbon source and argon as protector (argon/methane: 1/1). A 1 hour deposition time was sufficient to nearly fill the nanopipettes with carbon. The electrostatic discharge protection was used in all experiments to prevent damage to CNEs.[42] The

radius value was validated, and the electrode geometry was checked by transmission electron microscopy (TEM), using a JEOL JEM-2100 instrument.

Chemical modification of GCE/CNE surface. 4-Amino-2,2'-bipyridine (1 mM) molecule was converted to its corresponding diazonium salt using nitrosyl tetrafluoroborate (1.5 mM) in dry acetonitrile containing 0.1 M $TBABF_4$. The in situ generated diazonium salt was then electrochemically reduced for the grafting process in presence of 2,2-diphenyl-1-picrylhydrazyl (5 mM) to avoid multilayer formation as reported earlier.[36] ATR-FTIR spectra were obtained before and after modification (Figure S6). Characteristic bands (1300 − 1600 cm^{-1}) [43] of bpy were observed at the modified carbon surface. The attachment of copper was done using a reported procedure,[35] in which the modified electrode was immersed in DMF solution of copper nitrate overnight. The (bpy)Cu-modified electrode was washed with water before use. Highly stable and reproducible CVs were obtained with (bpy)Cu-GCE (Figure S7).

Supporting Information. Supplementary electrochemical data, CVs, current transients at CNE, Stability test, FTIR data, computational details, finite-element simulations of SECM experiments and COMSOL report.

ACKNOWLEDGMENTS

The support of this work by the National Science Foundation grant CHE-2247262 is gratefully acknowledged. This research used resources of the National Energy Research Scientific Computing Center, a DOE Office of Science User Facility supported by the Office of Science of the U.S. Department of Energy under Contract No. DE-AC02-05CH11231 using NERSC award BES-ERCAP0028088.

COMPETING INTERESTS STATEMENT

The authors declare that they have no conflict of interest.

REFERENCES

1. Barham, J. P.; König, B. Synthetic Photoelectrochemistry. *Angew. Chem., Int. Ed.* **2020**, *59*, 11732–11747.
2. Liu, J.; Lu, L.; Wood, D.; Lin, S. New redox strategies in organic synthesis by means of electrochemistry and photochemistry. *ACS Cent. Sci*. **2020**, *6,* 1317-1340.
3. Kalyanasundaram, K.; Grätzel, M. Photochemical Conversion and Storage of Solar Energy. *Photochem. Photobiol.* **1984**, 40, 807−822.
4. Lewis, N. S.; Nocera, D. G. Powering the Planet: Chemical Challenges in Solar Energy Utilization. *Proc. Natl. Acad. Sci. USA* **2006**, *103*, 15729-15735.
5. Kim, H.; Kim, H.; Lambert, T.; Lin, S. Reductive electrophotocatalysis: merging electricity and light to achieve extreme reduction potentials. *J. Am. Chem. Soc*. **2020**, *142*, 2087-2092.
6. Esswein, A. J.; Nocera, D. G. Hydrogen Production by Molecular Photocatalysis. *Chem. Rev.* **2007,** *107*, 4022-4047.
7. Artero, V.; Chavarot-Kerlidou, M.; Fontecave, M. Splitting Water with Cobalt. *Angew. Chem. Int. Ed.* **2011**, *50*, 7238–7266.
8. Pitman, C. L.; Miller, A. J. M. Molecular Photoelectrocatalysts for Visible Light-Driven Hydrogen Evolution from Neutral Water. *ACS Catal.* **2014**, *4*, 2727−2733.
9. Brereton, K. R.; Bonn, A. G.; Miller, A. J. M. Molecular Photoelectrocatalysts for Light-Driven Hydrogen Production. *ACS Energy Lett.* **2018**, *3*, 1128–1136.
10. Lee, Y.-M.; Nam, W.; Fukuzumi, S. Redox catalysis via photoinduced electron transfer. *Chem. Sci.* **2023**, *14*, 4205-4218.
11. Savéant, J.-M. Molecular Catalysis of Electrochemical Reactions. Mechanistic Aspects. *Chem. Rev.* **2008**, *108*, 2348−2378.
12. Yin, Q.; Tan, J. M.; Besson, C.; Geletii, Y. V.; Musaev, D. G.; Kuznetsov, A. E.; Luo, Z.; Hardcastleand, K. I.; Hill, C. L. A fast soluble carbon-free molecular water oxidation catalyst based on abundant metals. *Science* **2010**, *328*, 342–345.
13. Blakemore, J. D.; Crabtree, R. H.; Brudvig, G. W. Molecular Catalysts for Water Oxidation. *Chem. Rev.* **2015**, *115*, 12936-12973.
14. Gersten, S. W.; Samuels, G. J.; Meyer, T. J. Catalytic oxidation of water by an oxo-bridged ruthenium dimer. *J. Am. Chem. Soc.* **1982**, *104*, 4029–4030.
15. Concepcion, J. J.; Tsai, M. K.; Muckerman, J. T.; Meyer, T. J. Mechanism of water oxidation by single-site ruthenium complex catalysts. *J. Am. Chem. Soc.* **2010**, *132*, 1545–1557.
16. Yin, Q.; Tan, J. M.; Besson, C.; Geletii, Y. V.; Musaev, D. G.; Kuznetsov, A. E.; Luo, Z.; Hardcastleand, K. I.; Hill, C. L. A fast soluble carbon-free molecular water oxidation catalyst based on abundant metals. *Science* **2010**, *328*, 342–345.
17. Barnett, S. M.; Goldberg, K. I.; Mayer, J. M. A Soluble Copper–Bipyridine Water-Oxidation Electrocatalyst. *Nat. Chem*. **2012**, *4*, 498−502.
18. Joya, K. S., Subbaiyan, N. K., D'Souza, F. & de Groot, H. J. M. Surface-immobilized single-site iridium complexes for electrocatalytic water Splitting. *Angew. Chem., Int. Ed.* **2012**, *51*, 9601−9605.
19. Garrido-Barros, P., Gimbert-Surinach, C., Moonshiram, D., Picón, A., Monge, P., Batista, V. S. & Llobet, A. Electronic π- delocalization boosts catalytic water Oxidation by Cu(II) molecular catalysts heterogenized on graphene sheets. *J. Am. Chem. Soc.* **2017**, *139*, 12907−12910.

20. Li, X., Lei, H., Liu, J., Zhao, X., Ding, S., Zhang, Z., Tao, X., Zhang, W., Wang, W., Zheng, X. & Cao, R. Carbon nanotubes with cobalt corroles for hydrogen and oxygen evolution in pH 0−14 solutions. *Angew. Chem., Int. Ed.* **2018**, *57*, 15070−15075.
21. Hoque, Md. A., Gil-Sepulcre, M., de Aguirre, A., Elemans, J. A. A. W., Moonshiram, D., Matheu, R., Shi, Y., Benet-Buchholz, J., Sala, X., Malfois, M., Solano, E., Lim, J., Garzón-Manjón, A., Scheu, C., Lanza, M., Maseras, F., Gimbert-Suriñach, C. & Llobet, A. Water oxidation electrocatalysis using ruthenium coordination oligomers adsorbed on multiwalled carbon nanotubes. *Nat. Chem.* **2020**, *12*, 1060−1066.
22. Gil-Sepulcre, M., Linder, J. O., Schindler, D., Velasco, L., Moonshiram, D., Rüdinger, O., Stepanenko, V., Solano, E., Würthner, F. & Llobet, A. Surface promoted evolution of Ru-bda coordination oligomers boost the efficiency of water oxidation molecular electroanodes. *J. Am. Chem. Soc.* **2021**, *143*, 11651−11661.
23. Wu, L.; Nayak, A.; Shao, J.; Meyer, T. J. Crossing the bridge from molecular catalysis to a heterogenous electrode in electrocatalytic water oxidation. *Proc. Natl. Acad. Sci. USA* **2019**, **116**, 11153-11158.
24. Li, J.; Triana, C. A.; Wan, W.; Adiyeri Saseendran, D. P.; Zhao, Y.; Balaghi, S. E.; Heidari, S.; Patzke, G. R. Molecular and heterogeneous water oxidation catalysts: recent progress and joint perspectives. *Chem. Soc. Rev.* **2021**, *50*, 2444-2485.
25. Nong, H. N.; Falling, L. J.; Bergmann, A.; Klingenhof, M.; Tran, H. P.; Spöri, C.; Mom, R.; Timoshenko, J.; Zichittella, G.; Knop-Gericke, A.; Piccinin, S.; Pérez-Ramírez, J.; Cuenya, B. R.; Schlögl, R.; Strasser, P.; Teschner, D.; Jones, T. E. Key role of chemistry versus bias in electrocatalytic oxygen evolution. *Nature* **2020**, *587*, 408–413.
26. Boettcher, S. W.; Surendranath, Y. Heterogeneous electrocatalysis goes chemical. *Nat. Catal.* **2021**, *4*, 4–5.
27. Luo, S.-X. L.; Liu, R. Y.; Lee, S.; Swager, T. M. Electrocatalytic Isoxazoline−Nanocarbon Metal Complexes. *J. Am. Chem. Soc.* **2021**, *143*, 10441–10453.
28. Bates, J. S.; Biswas, S.; Suh, S.-E.; Johnson, M. R.; Mondal, B.; Root, T. W.; Stahl, S. S. Chemical and electrochemical O_2 reduction on earth-abundant M-N-C catalysts and implications for mediated electrolysis. *J. Am. Chem. Soc.* **2022**, *144*, 922-927.
29. Jackson, M. N.; Oh, S.; Kaminsky, C. J.; Chu, S. B.; Zhang, G.; Miller, J. T.; Surendranath, Y. Strong Electronic Coupling of Molecular Sites to Graphitic Electrodes via Pyrazine Conjugation. *J. Am. Chem. Soc.* **2018**, *140*, 1004–1010.
30. Jackson, M. N.; Surendranath, Y. Molecular control of heterogeneous electrocatalysis through graphite conjugation. *Acc. Chem. Res.* **2019**, *52*, 3432–3441.
31. Kaminsky, C. J.; Weng, S.; Wright, J.; Surendranath, Y. Adsorbed cobalt porphyrins act like metal surfaces in electrocatalysis *Nat. Catal.* **2022**, *5*, 430-442.
32. Barman, K.; Wang, X.; Jia, R.; Askarova, G.; Hu, G.; Mirkin, M. V. Voltage-driven molecular catalysis of electrochemical reactions. *J. Am. Chem. Soc.* **2021**, *143*, 17344−17347.
33. Barman, K.; Askarova, G.; Jia, R.; Hu, G.; Mirkin, M. V. Efficient Voltage-Driven Oxidation of Water and Alcohols by Organic Molecular Catalyst Directly Attached to a Carbon Electrode. *J. Am. Chem. Soc.* **2023**, *145*, 5786−5794.
34. Barman, K.; Chen, Y.; Wu, S.; Hu, G.; Mirkin, M. V. Voltage-Driven Molecular Catalysis: A Promising Approach to Electrosynthesis. *ACS Catal*. **2023**, *13*, 15869– 15876.

35. Zhou, X.; Zhang, T.; Abney, C. W.; Li, Z.; Lin, W. Graphene-immobilized Monomeric Bipyridine-M^{x+} (M^{x+} = Fe^{3+}, Co^{2+}, Ni^{2+}, or Cu^{2+}) Complexes for Electrocatalytic Water Oxidation. *ACS Appl. Mater. Interfaces* **2014**, *6*, 18475−18479.
36. Menanteau, T.; Levillain, E.; Downard, A.; Breton, T. Evidence of Monolayer Formation via Diazonium Grafting with a Radical Scavenger: Electrochemical, AFM and XPS Monitoring. *Phys. Chem. Chem. Phys.* **2015**, *17*, 13137−13142.
37. Menanteau, T.; Levillain, E.; Breton, T. Electrografting via Diazonium Chemistry: From Multilayer to Monolayer Using Radical Scavenger. *Chem. Mater.* **2013**, *25*, 2905–2909.
38. Jian, J. X.; Liao, J. X.; Zhou, M. H.; Yao, M. M.; Chen, Y. J.; Liang, X. W.; Liu, C. P.; Tong, Q. X. Enhanced Photoelectrochemical Water Splitting of Black Silicon Photoanode with pH-Dependent Copper-Bipyridine Catalysts. *Chem. − Eur. J.* **2022**, *28*, e202201520.
39. Gorantla, K. R.; Mallik, B. S. Three-Electron Two-Centered Bond and Single-Electron Transfer Mechanism of Water Splitting via a Copper–Bipyridine Complex. *J. Phys. Chem. A* **2023**, *127*, 160–168.
40. Iwamura, M.; Takeuchi, S.; Tahara, T. Ultrafast Excited-State Dynamics of Copper(I) Complexes. *Acc. Chem. Res.* **2015**, *48*, 782−791.
41. Li, Y.; Hu, K.; Yu, Y.; Rotenberg, S. A.; Amatore, C.; Mirkin, M. V. Direct electrochemical measurements of reactive oxygen and nitrogen species in nontransformed and metastatic human Breast Cells. *J. Am. Chem. Soc.* **2017**, *139*, 13055−13062.
42. Nioradze, N.; Chen, R.; Kim, J.; Shen, M.; Santhosh, P.; Amemiya, S. Origins of nanoscale damage to glass-sealed platinum electrodes with submicrometer and nanometer size. *Anal. Chem.* **2013**, *85*, 6198−6202.
43. Gerasimova, T. P.; Katsyuba, S. A. Bipyridine and phenanthroline IR-spectral bands as indicators of metal spin state in hexacoordinated complexes of Fe(II), Ni(II), and Co(II). *Dalton Trans.* **2013**, *42*, 1787−1797.

For TOC only

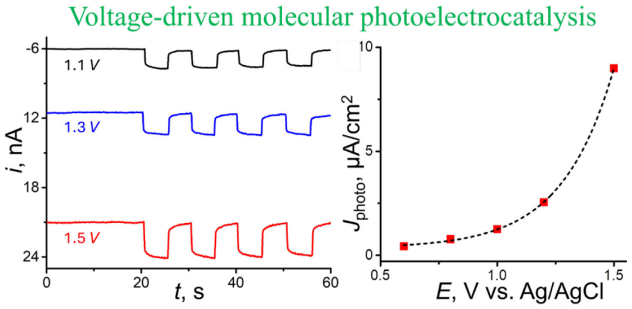
Voltage-driven molecular photoelectrocatalysis
1.1 V
1.3 V
1.5 V
i, nA
-6
12
18
24
0
20
40
60
t, s
J_photo, μA/cm²
10
5
0
0.5
1.0
1.5
E, V vs. Ag/AgCl